PHILOSOPHICAL TRANSACTIONS OF THE ROYAL SOCIETY A

Phil. Trans. R. Soc. A (2008) **366**, 4239–4252
doi:10.1098/rsta.2008.0071
Published online 30 September 2008

Compressibility of water in magma and the prediction of density crossovers in mantle differentiation

By Carl B. Agee*

Institute of Meteoritics, and Department of Earth and Planetary Sciences, University of New Mexico, Albuquerque, NM 87131, USA

Hydrous silicate melts appear to have greater compressibility relative to anhydrous melts of the same composition at low pressures (<2 GPa); however, at higher pressures, this difference is greatly reduced and becomes very small at pressures above 5 GPa. This implies that the pressure effect on the partial molar volume of water in silicate melt ($\partial \bar{V}_{H_2O}/\partial P$) is highly dependent on pressure regime. Thus, H_2O can be thought of as the most compressible 'liquid oxide' component in silicate melt at low pressure, but at high pressure its compressibility resembles that of other liquid oxide components. A best-fit curve to the data on $\bar{V}_{H_2O}$ from various studies allows calculation of hydrous melt compression curves relevant to high-pressure planetary differentiation. From these compression curves, crystal–liquid density crossovers are predicted for the mantles of the Earth and Mars. For the Earth, trapped dense hydrous melts may reside atop the 410 km discontinuity, and, although not required to be hydrous, atop the core–mantle boundary (CMB), in accord with seismic observations of low-velocity zones in these regions. For Mars, a density crossover at the base of the upper mantle is predicted, which would produce a low-velocity zone at a depth of approximately 1200 km. If perovskite is stable at the base of the Martian mantle, then density crossovers or trapped dense hydrous melts are unlikely to reside there, and long-lived, melt-induced, low-velocity regions atop the CMB are not predicted.

Keywords: mantle differentiation; magma ocean; high pressure; water

1. Introduction

'Density crossovers' occur between silicate liquids and their coexisting equilibrium crystalline phases when compression curves of the liquids and the crystals intersect at high pressure. This can occur between certain crystal–liquid pairs because the compressibilities of silicate liquids are higher than those of silicate crystals, and at high enough pressures the compression curves 'cross over'. This phenomenon has been confirmed experimentally by numerous studies over the past 25 years (Rigden *et al.* 1984, 1989; Agee & Walker 1988*b*, 1993;

*agee@unm.edu

One contribution of 14 to a Discussion Meeting Issue 'Origin and differentiation of the Earth: past to present'.

Miller *et al.* 1991*a*; Suzuki *et al.* 1995; Circone & Agee 1996; Smith & Agee 1997; Agee 1998; Ohtani & Maeda 2001). There are also examples in geologically interesting systems where silicate crystals float in their equilibrium silicate liquids at 1 bar, such as plagioclase flotation in lunar basalt (Walker & Hays 1977) and flotation of liquidus olivine in melts on the forsterite–fayalite join (Herzberg *et al.* 1982); however, these will not be discussed further in this paper, and I will focus only on crystal flotation due to high pressure.

Density crossovers may have important implications for the Earth and planetary differentiation scenarios (Stolper *et al.* 1981; Nisbet & Walker 1982; Herzberg 1984; Ohtani 1984, 1985; Agee & Walker 1988*a*; Delano 1990; Miller *et al.* 1991*b*), especially within a magma ocean environment, where temperatures are assumed to be high enough for wholesale melting of anhydrous mantle to occur at great depths and very high pressures. For the modern Earth, with a more modest geotherm, deep mantle melting is probably restricted to heterogeneous regions with thermal boundary layers such as the core–mantle boundary (CMB) and its proposed ultra-low-velocity zones (ULVZ; Williams & Garnero 1996; Vidale & Hedlin 1998; Berryman 2000; Rost *et al.* 2005) or regions where the mantle solidus has been lowered by the presence of water such as atop the 410 km discontinuity (Nolet & Zielhuis 1994; Revenaugh & Sipkin 1994; Bercovici & Karato 2003; Leahy & Bercovici 2007; Toffelmier & Tyburczy 2007).

Hydrous density crossovers are not predictable from experimental data on anhydrous melts. For example, we expect that the density of hydrous melts will be lower than for anhydrous melts (Ochs & Lange 1999), but the details of whether hydrous melts will be more compressible with a smaller isothermal bulk modulus (K_T), or whether the pressure effect on the bulk modulus (K') will be the same, or larger or smaller, need independent experimental testing. How any of these differences will affect the location of density crossovers also needs confirmation. To answer these questions, I refer to three recent experimental studies that address the issue of hydrous melt density and compressibility at high pressure (Matsukage *et al.* 2005; Sakamaki *et al.* 2006; Agee 2008), and pioneering work on hydrous melts and glasses at low pressure (Burnham & Davis 1971; Ochs & Lange 1999). From these data, I derive the effect of pressure on the partial molar volume of H_2O in silicate melt ($\bar{V}_{H_2O}$) and predict the existence of crystal–liquid density crossovers for hydrous magmas in the mantles of the Earth and Mars.

2. Partial molar volume of water in silicate liquid at high pressure

Bottinga & Weill (1970) showed that partial molar volumes of silicate liquids can be treated as constants over a compositional range of 40–80 mol% SiO_2, although data on linear mixing at high pressure are, at this time, incomplete. Therefore, the density (ρ) of a silicate liquid can be expressed as

$$\rho = \sum_i \frac{X_i M_i}{X_i \bar{V}_i},$$

where X_i is the mole fraction of component i; $\bar{V}_i$ is its partial molar volume; and M_i is its gram formula weight (gfw; also relative molar mass). The components are also referred to as 'liquid oxides' and include SiO_2, Al_2O_3, FeO, MgO, CaO,

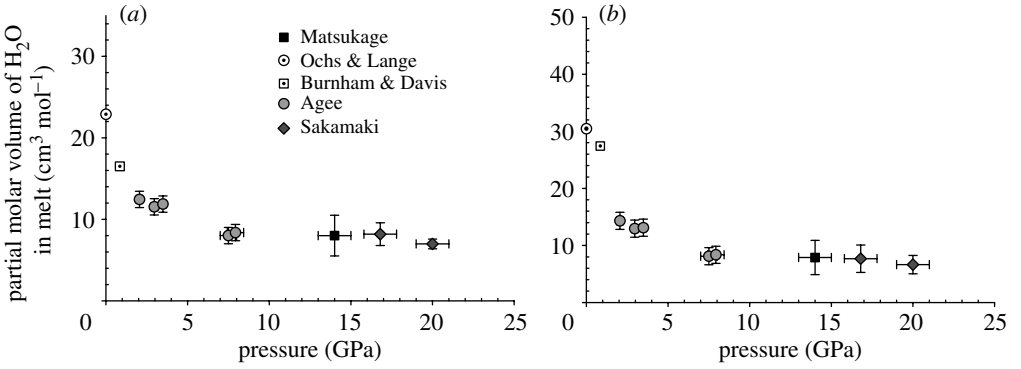

Figure 1. (*a*) Pressure versus $\bar{V}_{H_2O}$ diagram summarizing data from various experimental studies (Burnham & Davis 1971; Ochs & Lange 1999; Matsukage *et al.* 2005; Sakamaki *et al.* 2006; Agee 2008) that measured the density of hydrous silicate glasses and liquids. The experiments were performed over a wide temperature range (800–2300°C) and are uncorrected for the effect of thermal expansion on $\bar{V}_{H_2O}$. The data point of Matsukage is from their estimate of $\bar{V}_{H_2O}$ based on four experiments at 1900°C and $p=10$–16.2 GPa. See table 1 for details. (*b*) Pressure versus $\bar{V}_{H_2O}$ diagram with the data from (*a*) normalized to 1800°C using the effect of thermal expansion on $\bar{V}_{H_2O}$ at high pressure from Burnham & Davis (1971) (see text). The Ochs & Lange (1999) 1 bar density was corrected for thermal expansion with $\partial\bar{V}_{H_2O}/\partial P = 0.00946\ \mathrm{cm^3\ mol^{-1}\ K^{-1}}$.

Na_2O, etc. In hydrous silicate liquids, H_2O can also be considered as one of the dissolved liquid oxide components. Therefore, the difference between the density of anhydrous silicate liquid and hydrous silicate liquid of the same composition at P and T is determined by the value of the partial molar volume of water and its mole fraction in the hydrous liquid.

Figure 1*a* shows data from various studies that measured the density of hydrous silicate liquids or glasses at low and high pressures, and from which we cite or derive values for $\bar{V}_{H_2O}$, uncorrected for thermal expansion. The experimental densities were measured on hydrous silicate glasses near the glass transition temperature at 1 bar with dilatometry (Ochs & Lange 1999), on hydrous albite melt up to 0.85 GPa in an internally heated, gas pressurized, P–V–T vessel (Burnham & Davis 1971), on hydrous FeO-rich komatiite melt at 1.5–9 GPa in a piston–cylinder and multi-anvil apparatus using the sink/float technique (Agee 2008), on hydrous FeO-rich ultrabasic melt at 10–16 GPa (Matsukage *et al.* 2005) and on molten hydrous mid-ocean ridge basalts (MORB) (Sakamaki *et al.* 2006) in a multi-anvil apparatus using the sink/float technique. The highest temperatures (2300°C) were in the high-pressure data from Sakamaki *et al.* (2006) and the lowest temperatures (800°C) were from Burnham & Davis (1971). The values of $\bar{V}_{H_2O}$ from Burnham & Davis (1971) and Ochs & Lange (1999) are adopted directly from their tables and graphs, whereas those from Sakamaki *et al.* (2006) and Agee (2008) are derived from the difference in density between anhydrous and hydrous liquids of the same composition, respectively, at high P and T, using the relationship

$$\bar{V}_{H_2O}^{P,T} = \left\{ \left[\left(\sum_i X_i M_i + X_{H_2O} M_{H_2O} \right) \Big/ \rho_{hyd}^{P,T} \right] - \sum_i X_i \bar{V}_i^{P,T} \right\} \Big/ X_{H_2O},$$

where $\sum_i \bar{V}_i^{P,T} = \sum_i (M_i X_i / \rho_{anhyd}^{P,T} X_i)$ and $\sum_i X_i = 1 - X_{H_2O}$.

Table 1. Data from various experiments (see text and figure 1 for full references).

experiment	source	pressure (GPa)	temp (°C)	$\rho^{P,T}_{\mathrm{anhyd}}$ (g cm^{-3})	$\rho^{P,T}_{\mathrm{hyd}}$ (g cm^{-3})	$X_{\mathrm{H_2O}}$ (mol. fract.)	X_i (mol. fract.)	$M_{\mathrm{H_2O}}$ (gfw mol. fract.)	M_i (gfw mol. fract.)	$\bar{V}_i^{P,T}$ (cm^3 mol^{-1})	$\bar{V}_{\mathrm{H_2O}}^{P,T}$ (cm^3 mol^{-1})	$\bar{V}_{\mathrm{H_2O}}^{P,1800}$ (cm^3 mol^{-1})
diamond in MORB melt	Sakamaki *et al.*	16.8	2300	3.598	3.550	0.066	0.934	1.19	58.20	16.18	8.18	7.67
diamond in MORB melt	Sakamaki *et al.*	20.0	2200	3.743	3.580	0.231	0.769	4.16	47.93	12.80	6.97	6.63
diamond in Fe-rich silicate melts	Matsukage *et al.*	14.0	1900	n.a.	n.a.	n.a.	n.a.	n.a.	n.a.	n.a.	8.00	7.88
garnet in Fe-rich komatiite melt	Agee	7.9	1800	3.72	3.663	0.066	0.934	1.19	58.03	15.60	8.37	8.37
garnet in Fe-rich komatiite melt	Agee	7.5	1750	3.695	3.645	0.066	0.934	1.19	58.03	15.71	8.00	8.11
olivine in Fe-rich komatiite melt	Agee	3.49	1500	3.45	3.207	0.156	0.844	2.81	52.54	15.23	11.87	13.10
olivine in Fe-rich komatiite melt	Agee	2.96	1500	3.413	3.188	0.156	0.844	2.81	52.54	15.39	11.54	12.95
olivine in Fe-rich komatiite melt	Agee	2.05	1500	3.341	3.099	0.156	0.844	2.81	52.54	15.73	12.44	14.32
hydrous albite melt	Burnham & Davis	0.85	950	n.a.	n.a.	n.a.	n.a.	n.a.	n.a.	n.a.	16.50	27.42
hydrous glasses	Ochs & Lange	0.0001	1000	n.a.	n.a.	n.a.	n.a.	n.a.	n.a.	n.a.	22.90	30.46

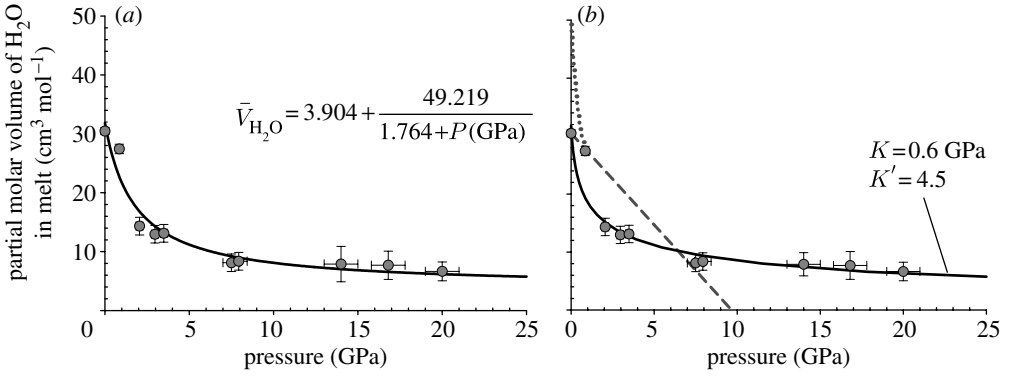

Figure 2. Pressure versus $\bar{V}_{H_2O}$ diagrams showing best fits to the data described by (*a*) a three-parameter hyperbolic decay curve and (*b*) the Vinet equation (solid curve), normalized to 1800°C. Also shown in (*b*) are earlier estimates of $\partial \bar{V}_{H_2O}/\partial P$ from Burnham & Davis (1971) (dotted curve) and Ochs & Lange (1999) (dashed curve).

This was possible since both studies reported experimentally measured values of anhydrous and hydrous liquids of the same composition, which is a highly effective approach to the determination of $\bar{V}_{H_2O}$ at high pressure. Matsukage *et al.* (2005) did not measure the density of the anhydrous versions of their experimental liquids, and therefore we adopt the 'estimated' value of $\bar{V}_{H_2O}$ from that paper and assign the largest error bars to it. Grouping these data together implies that $\bar{V}_{H_2O}$ does not depend on silicate liquid composition, total water content and water speciation. This has been demonstrated by Ochs & Lange (1999) for polymerized and depolymerized silicate liquids, although it would be desirable to test this hypothesis over a wider melt composition range.

In figure 1*b*, I apply a correction for thermal expansion on $\bar{V}_{H_2O}$ from Burnham & Davis (1971), i.e.

$$\bar{V}^{1800}_{H_2O} = \bar{V}^{T}_{H_2O} - \Delta T \frac{\mathrm{d}\bar{V}_{H_2O}}{\mathrm{d}T},$$

where $\mathrm{d}\bar{V}_{H_2O}/\mathrm{d}T = 0.0178/(0.813 + P(\mathrm{GPa}))$ and normalize the data to 1800°C. Because the thermal expansion of $\bar{V}_{H_2O}$ is assumed to decrease significantly with pressure, the corrected values at pressures above 10 GPa are very similar to the uncorrected values. On the other hand, the low-pressure and low-temperature data show a much larger difference in $\bar{V}_{H_2O}$ when corrected to 1800°C. Regardless of whether a thermal expansion correction is made or not, the data in figure 1*a*,*b* show a very strong pressure dependence for $\bar{V}_{H_2O}$ at pressures from 1 bar to approximately 3 GPa. Somewhere between approximately 3 and 7 GPa the change in $\bar{V}_{H_2O}$ with pressure decreases markedly. At pressures above 7 GPa, $\bar{V}_{H_2O}$ appears to change only very slightly with pressure. Table 1 gives all the data from the various studies discussed here.

The $\bar{V}_{H_2O}$ data are shown in figure 2*a* best-fitted to a three-parameter hyperbolic decay curve of the form

$$f = y_0 + \frac{ab}{b + x},$$

or, with fitted parameters,

$$\bar{V}_{H_2O}^{1800,P} = 3.904 + \frac{27.905 \times 1.764}{1.764 + P(\mathrm{GPa})}.$$

The best-fit curve intersects, within error bars, all the $\bar{V}_{H_2O}$ data points and describes well the very strong pressure effect on $\bar{V}_{H_2O}$ in the range 0–3 GPa and the weak pressure effect above 7 GPa. At very high pressures, the curve shows that $\bar{V}_{H_2O}$ is decreasing very slightly with pressure and approaches 3.904 $\mathrm{cm^3\ mol^{-1}}$ as $P \rightarrow \infty$. This suggests that the compressibility of H_2O in magma has a distinctly different character at low pressure than at high pressure. At low pressure (0–3 GPa), H_2O is highly compressible compared with other silicate melt components; however, at high pressures above 7 GPa, H_2O compressibility is comparable with that of the other liquid oxides (Bottinga & Weill 1970; Lange & Carmichael 1987) that make up silicate melts. This hyperbolic decay curve is similar in shape to the Vinet equation (Vinet *et al.* 1989) fit to $\bar{V}_{H_2O}$ reported by Sakamaki *et al.* (2006), which was constrained by fewer data points. I also fit the data to the Vinet equation given by

$$P = 3K_T \left(\frac{\bar{V}_{H_2O}^{P,T}}{\bar{V}_{H_2O}^{0,T}}\right)^{-2/3} \left[1 - \left(\frac{\bar{V}_{H_2O}^{P,T}}{\bar{V}_{H_2O}^{0,T}}\right)^{1/3}\right] \exp\left\{\frac{3}{2}(K' - 1)\left[1 - \left(\frac{\bar{V}_{H_2O}^{P,T}}{\bar{V}_{H_2O}^{0,T}}\right)^{1/3}\right]\right\},$$

and derive values for the isothermal bulk modulus (K_T) of 0.6 GPa with pressure derivative (K') of 4.5. Figure 2*b* shows that the Vinet fit is nearly identical to the hyperbolic decay curve up to 25 GPa, except that it is slightly steeper between 0 and 3 GPa. Extrapolation to much greater than 25 GPa reveals that the Vinet equation gives values for $\bar{V}_{H_2O}$ that are significantly smaller than the hyperbolic decay curve for lower mantle pressures. As I discuss in a later section, this could be incorrect, as it produces the unexpected outcome that hydrous melt becomes denser than anhydrous melts of the same composition at very high pressure. Figure 2*b* also shows earlier attempts at predicting $\partial \bar{V}_{H_2O}/\partial P$ from Burnham & Davis (1971) and Ochs & Lange (1999). Because there was an absence of high-pressure data at the time when these pioneering studies were done, they were unable to capture the very strong change in the slope of $\partial \bar{V}_{H_2O}/\partial P$.

3. Prediction of density crossovers in hydrous mantle differentiation

Our best-fit curve to the data in figure 2*a* allows estimation of $\bar{V}_{H_2O}^{P}$ and calculation of hydrous magma density at high pressures ($\rho_{hyd}^{P,T}$) within the mantles of the terrestrial planets. This can be accomplished by assuming we have data on anhydrous magma with values for K_T and K' (e.g. Agee 1998) and a 1 bar reference density ($\rho_{anhyd}^{0,T}$; Lange & Carmichael 1987). To calculate the high-pressure density of the hydrous magma ($\rho_{hyd}^{P,T}$), I first calculate the high-pressure density of anhydrous magma ($\rho_{anhyd}^{P,T}$) using the third-order Birch–Murnaghan equation,

$$P = \frac{3}{2}K_T \left[\left(\frac{\rho_{anhyd}^{P,T}}{\rho_{anhyd}^{0,T}}\right)^{7/3} - \left(\frac{\rho_{anhyd}^{P,T}}{\rho_{anhyd}^{0,T}}\right)^{5/3}\right] \left\{1 - \frac{3}{4}(4 - K')\left[\left(\frac{\rho_{anhyd}^{P,T}}{\rho_{anhyd}^{0,T}}\right)^{2/3} - 1\right]\right\}.$$

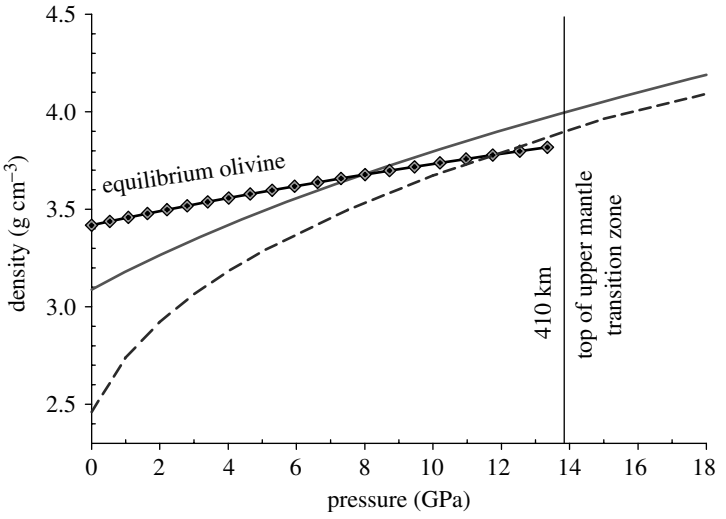

Figure 3. Pressure versus density diagram relevant to the Earth's upper mantle, normalized to 1800°C, showing anhydrous (solid) and hydrous (dashed) compression curves for FeO-rich komatiite. Also shown is the compression curve for liquidus olivine (Fo64). The anhydrous komatiite and olivine curves are calculated using the Birch–Murnaghan equation. The hydrous curve is derived from the three-parameter hyperbolic decay curve describing $\partial \bar{V}_{H_2O}/\partial P$ and the anhydrous compression curve. The diagram illustrates that hydrous silicate melt has a density crossover with coexisting liquidus olivine above the 410 km discontinuity.

Then I take

$$\rho^{P,T}_{\text{anhyd}} = \sum_i \frac{X_i M_i}{X_i \bar{V}^{P,T}_i} \quad \text{and} \quad \rho^{P,T}_{H_2O} = \frac{X_{H_2O} M_{H_2O}}{X_{H_2O} \bar{V}^{P,T}_{H_2O}},$$

to calculate

$$\rho^{P,T}_{\text{hyd}} = \sum_i \frac{X_i M_i + X_{H_2O} M_{H_2O}}{X_i \bar{V}^{P,T}_i + X_{H_2O} \bar{V}^{P,T}_{H_2O}},$$

where $\sum_i X_i = 1 - X_{H_2O}$.

Figure 3 shows compression curves for an FeO-rich komatiite that could represent a partial melt in the upper mantle. The density of the anhydrous version of this melt has been measured at high pressure (Agee 2008), and the compression curve is calculated from the Birch–Murnaghan equation with a bulk modulus $K_{1800} = 30$ GPa and $K' = 4$. I apply the method discussed above, using $\bar{V}^{1800,P}_{H_2O} = 3.904 + (27.905 \times 1.764)/(1.764 + P(\text{GPa}))$, to construct a compression curve of the hydrous version of this komatiite with 5 wt% H_2O by calculating its density over a range of pressure from 0 to 18 GPa. At low pressures, the hydrous komatiite compression curve has a steeper slope than the anhydrous curve, but at $p > 10$ GPa the two curves have similar slopes, which is due to the effect of pressure on $\partial \bar{V}_{H_2O}/\partial P$ as discussed above. Also shown in figure 3 is a calculated compression curve for olivine that is likely to be on the liquidus of the FeO-rich komatiite. The olivine compression curve intersects the anhydrous komatiite curve at approximately 8 GPa, resulting in a crystal–liquid density crossover. This anhydrous density crossover is consistent with the olivine flotation hypothesis confirmed in several earlier studies cited in §1. The olivine compression curve

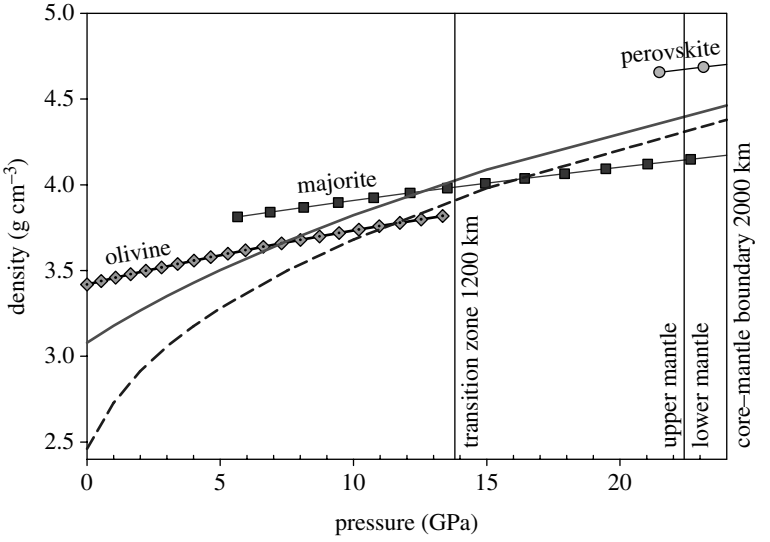

Figure 4. Pressure versus density diagram relevant to the entire mantle of Mars, normalized to 1800°C, with the same compression curves (solid, Fe-rich komatiite; dashed, Fe-rich komatiite with 5 wt% H_2O) as shown in figure 3, showing that a density crossover between hydrous silicate melt and olivine could exist at a depth just above the 1200 km transition zone boundary. A density crossover with liquidus majorite garnet is predicted to occur within the transition zone; however, no density crossover exists that would cause silicate melt to become denser than perovskite atop the Martian CMB. Depths are from Bertka & Fei (1998).

intersects the hydrous komatiite curve at approximately 12 GPa or 360 km depth in the Earth, indicating that olivine will float in a melt with up to 5 wt% H_2O above the 410 km discontinuity in the Earth's upper mantle. This predicted olivine–hydrous melt density crossover is in good agreement with the water filter hypothesis (Bercovici & Karato 2003), in which negatively buoyant hydrous melts are formed and trapped above the 410 km discontinuity from a dehydration reaction caused by the wadsleyite → olivine phase transformation. It appears from figure 3 that water contents above 5 wt%, at approximately 6–7 wt%, cause olivine to become negatively buoyant atop the transition zone. This is a relatively high water content that is unlikely to be required in the water filtration model or to explain seismic low-velocity regions, and the main point of figure 3 is that crystal–liquid density crossovers can exist at upper mantle pressures when significant amounts of water are dissolved in magma.

In figure 4, I apply these same data to the mantle of Mars and illustrate the density–pressure–depth relationships between anhydrous FeO-rich komatiite, FeO-rich komatite with 5 wt% H_2O and possible liquidus crystalline phases olivine, majorite garnet and perovskite. A density crossover exists for hydrous silicate melt and olivine atop the mantle transition zone, which in Mars occurs at approximately 1200 km depth (approx. 14 GPa). This could mean that a region of low seismic velocity exists at 1200 km in Mars, analogous to the low S-wave velocities observed atop the 410 km discontinuity in the Earth (Revenaugh & Sipkin 1994), which may be associated with the presence of negatively/neutrally buoyant hydrous melts (Bercovici & Karato 2003). The depth of the CMB in Mars is not well known because we have no seismic velocity profiles for the Martian interior. However,

estimates based on moment of inertia (Yoder *et al.* 2003) and phase equilibria experiments (Bertka & Fei 1998) support the possibility that the top of a sulphur-rich Martian core would be at a pressure of approximately 24 GPa or a depth of approximately 2000 km. If so, then there will be a narrow 'lower mantle' layer that is rich in $(Mg,Fe)SiO_3$ perovskite, and perovskite will probably be the liquidus phase atop the Martian CMB. In this case, as shown in figure 4, both anhydrous and hydrous melts will be positively buoyant in the lower mantle layer. Thus, melts, if they are generated by CMB thermal boundary-layer anomalies, will tend not to be trapped or reside in this layer for a long time, but will instead rise upwards. This is in contrast to the possibility of dense trapped melts existing atop the Earth's CMB, which I discuss below. It is worth noting that majorite garnet becomes the liquidus phase at approximately 22 GPa, approximately 200 km above the Martian CMB, and it would float in hydrous melt at this depth up to the level of approximately 16 GPa or 1300 km depth, in other words, a region approximately 500 km thick in the Martian transition zone. If there is appreciable water in the Martian interior, and if significant thermal anomalies can exceed the hydrous mantle solidus, and extend up into the transition zone, then hydrous melts there will be negatively buoyant relative to the coexisting crystalline majorite garnets, forming a ULVZ at 1300–1800 km depth in Mars.

4. Extrapolation of $\bar{V}_{H_2O}$ to lower mantle pressures

The data for $\bar{V}_{H_2O}$ in table 1 and figures 1 and 2 cover pressures up to approximately 20 GPa. This now allows reliable prediction of hydrous magma density in the Earth's upper mantle and the transition zone, as discussed above. On the other hand, there is considerable interest in the possibility of melting at the base of the Earth's lower mantle; thus, I consider the extrapolation of the current data to pressures of approximately 140 GPa, which is approximately the pressure at the CMB. Figure 5 shows that the three-parameter hyperbolic decay curve and the Vinet equation fits to the data give diverging extrapolation trajectories (figure 6). The three-parameter hyperbolic decay curve gives higher values for $\bar{V}_{H_2O}$ (approx. 4 $cm^3\,mol^{-1}$) at the pressure equivalent to the CMB, while the Vinet equation gives $\bar{V}_{H_2O} \simeq 2\ cm^3\,mol^{-1}$. We see some unexpected relationships at $p > 30$ GPa when we compare the anhydrous komatiite compression curve to the two hydrous compression curves derived from the two different $\partial\bar{V}_{H_2O}/\partial P$ extrapolations. The three-parameter hyperbolic decay curve hydrous $\partial\bar{V}_{H_2O}/\partial P$ extrapolation produces a compression curve that diverges from the anhydrous curve, showing increasing '$\Delta\rho$' with pressure in the range 30–150 GPa (figure 7), whereas the data at less than 20 GPa indicate that $\Delta\rho$ decreases significantly with P at low pressure and is approximately constant above 10 GPa. The divergence of the three-parameter hyperbolic decay curve could possibly be an extrapolation artefact; however, data at pressures above 30 GPa are needed to test this. Diverging anhydrous and hydrous compression curves may not be impossible. It simply requires that $\bar{V}_{H_2O}$ decreases with pressure at a lesser rate than the sum of the partial molar volumes of the other oxide components in the melt. Why this should happen in the lower mantle and not in the upper mantle may not have a logical explanation and, I stress, may be an artefact of the three-parameter hyperbolic decay curve.

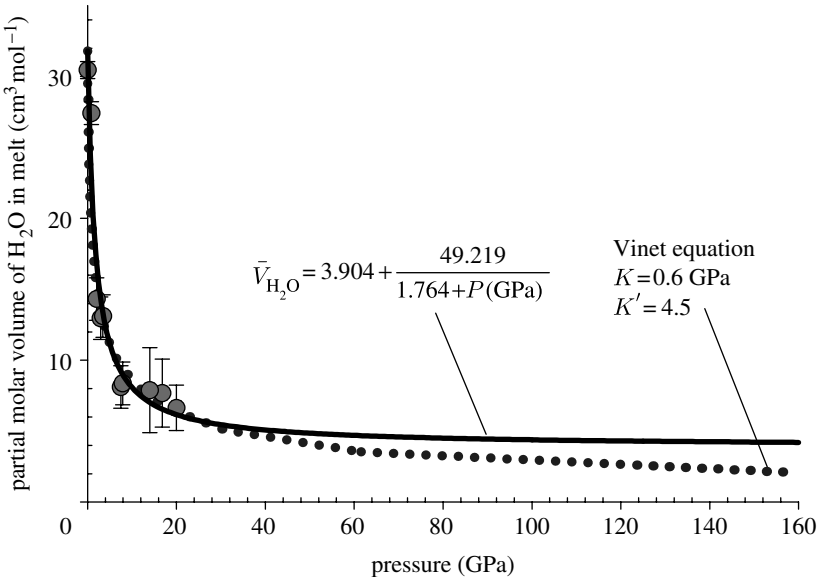

Figure 5. Pressure versus $\bar{V}_{H_2O}$ diagram (normalized to 1800°C) showing the extrapolations of the best-fit equation-of-state curves to lower mantle pressures. The three-parameter hyperbolic decay curve is solid and the Vinet equation is dotted.

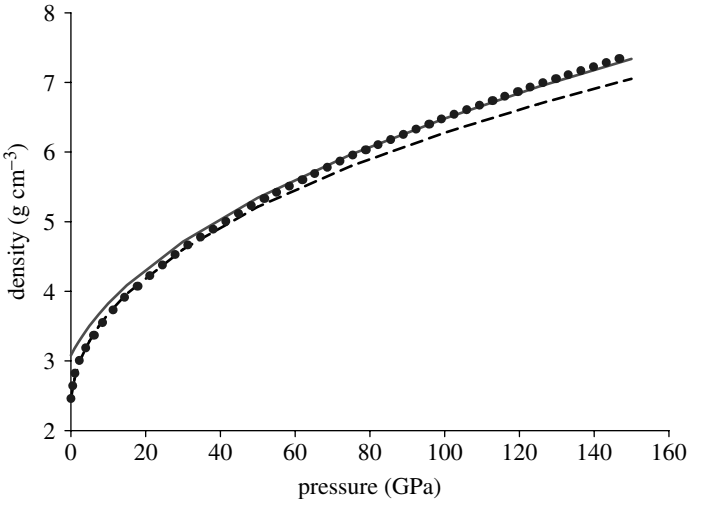

Figure 6. Pressure versus density diagram (normalized to 1800°C) comparing two compression curves for hydrous silicate melt (FeO-rich komatiite, 1800°C) and one for anhydrous silicate melt of the same composition. The hydrous compression curve (dashed) derived from $\partial \bar{V}_{H_2O}/\partial P$ given by the best-fit three-parameter hyperbolic decay curve converges with the anhydrous curve (solid, $K = 30$ GPa, $K' = 4$) up to approximately 30 GPa and then diverges at higher pressures. The hydrous compression curve (dotted) derived from $\partial \bar{V}_{H_2O}/\partial P$ given by the Vinet equation converges with the anhydrous curve (solid) and crosses over at approximately 90 GPa.

The Vinet equation extrapolation gives the opposite effect, in that it produces a hydrous compression curve that converges with the anhydrous curve. Convergence is consistent with the data-constrained part of the curve at less than 20 GPa, but the

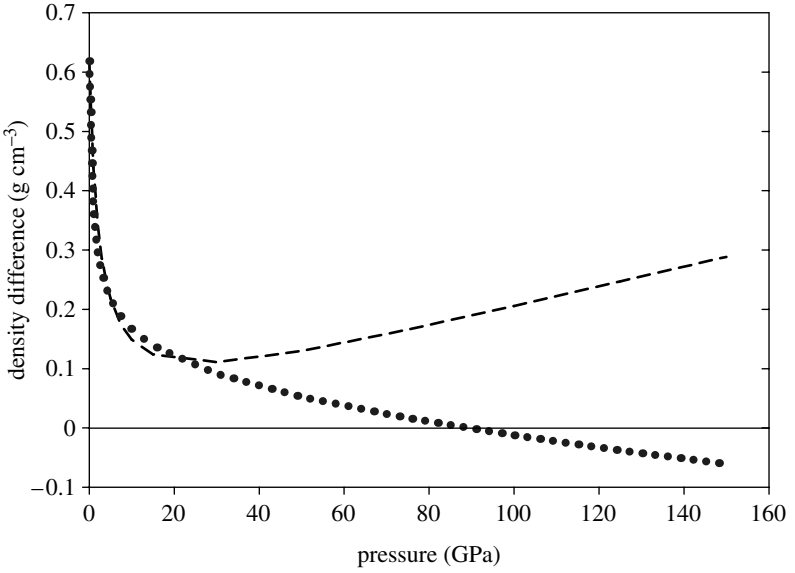

Figure 7. Pressure versus density difference (anhydrous minus hydrous, $\Delta\rho$) between hydrous compression curves and the anhydrous compression curve shown in figure 6. This diagram (normalized to 1800°C) illustrates the divergence and convergence (with crossover, $\Delta\rho=0$) derived from two different $p-\bar{V}_{H_2O}$ best-fit equations of state (dashed curve, $\bar{V}_{H_2O}$ from decay fit; dotted curve, $\bar{V}_{H_2O}$ from Vinet equation) described in the text.

Vinet-derived convergence results in a density crossover with anhydrous melt at 90 GPa, where $\Delta\rho$ is zero and at high pressures becomes negative (figure 7). This may seem at first glance to be a 'forbidden' outcome; however, it simply requires that $\bar{V}_{H_2O}$ decreases with pressure at a greater rate than the sum of the partial molar volumes of the other oxide components in the melt. This is indeed observed at $p<20$ GPa; however, the question remains open if this is an extrapolation artefact or if hydrous melts can become denser than anhydrous melts. Clearly, these questions cannot be adequately addressed until new experimental data on $\bar{V}_{H_2O}$ at lower mantle pressures are available. Perhaps a more likely outcome is that the hydrous and anhydrous curves continue to converge at pressures above 30 GPa; however, the convergence becomes very small and the curves would be indistinguishable from parallel. Even though these examples demonstrate some of the uncertainties in extrapolating upper mantle data to pressures of the deep lower mantle, and the need for new data at higher pressures, I now apply the current extrapolations and explore the possibility of density crossovers in the lower mantle.

Figure 8 shows the density–pressure relationships for anhydrous FeO-rich komatiite melt, hydrous FeO-rich komatiite melt with 5 wt% H_2O and crystalline $(Mg,Fe)SiO_3$ perovskite in the Earth's lower mantle. I show two versions of the hydrous compression curve as follows. The first one is a compression curve that diverges from the anhydrous curve at $p>30$ GPa, and is derived from the best-fit three-parameter hyperbolic decay for $\bar{V}_{H_2O}$. The other is a compression curve that converges with and crosses over the anhydrous curve at 90 GPa, and is derived from the best-fit Vinet equation for $\bar{V}_{H_2O}$. The anhydrous melt compression curve has a density crossover with perovskite at 95 GPa, which is consistent with earlier

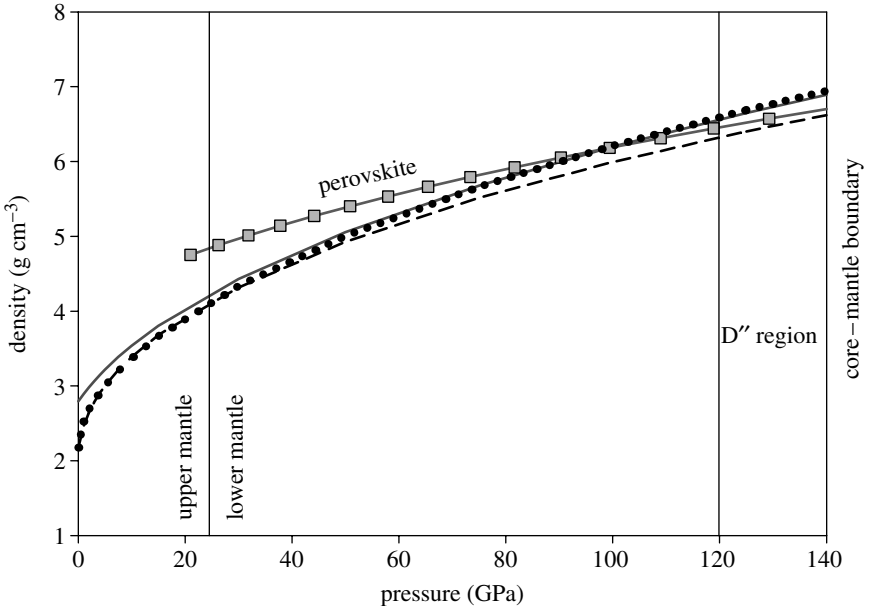

Figure 8. Pressure versus density diagram (normalized to 3000°C) showing possible crystal–liquid density crossovers in the Earth's lower mantle, for hydrous and anhydrous melts and liquidus perovskite (solid curve, Fe-rich komatiite melt; dashed curve, diverging hydrous melt; dotted curve, converging hydrous melt). The perovskite (EN76) compression curve was calculated with the Birch–Murnaghan equation and elastic constants from Bertka & Fei (1998).

predictions (Miller *et al.* 1991*b*; Agee 1998). For the divergent hydrous compression curve, the density crossover with perovskite occurs at $p > 140$ GPa. In this case, silicate melt with 5 wt% water would be less dense than perovskite atop the CMB; however, melts with lower water contents (<5 wt%) could be neutrally buoyant or denser than coexisting perovskite at the CMB. For the convergent hydrous curve, the crossover with perovskite is slightly lower than 95 GPa and, of course, at a lower pressure than the anhydrous curve. As a result, the density crossover for both anhydrous and hydrous melts and equilibrium perovskite occurs at similar pressures at the base of the lower mantle or in the D″ layer. This is consistent with the observed seismic ULVZ (Williams & Garnero 1996), thought to be associated with partial melts trapped by negative buoyancy at these depths, although these melts are not required to be hydrous.

This work is supported by grants from NSF EAR and NASA. Comments and suggestions by Jed Mosenfelder improved the manuscript.

References

Agee, C. B. 1998 Crystal–liquid density inversions in terrestrial and lunar magmas. *Phys. Earth Planet. Inter.* **107**, 63–74. (doi:10.1016/S0031-9201(97)00124-6)

Agee, C. B. 2008 Static compression of hydrous silicate melt and the effect of water on planetary differentiation. *Earth Planet. Sci. Lett.* **265**, 641–654. (doi:10.1016/j.epsl.2007.11.010)

Agee, C. B. & Walker, D. 1988*a* Mass balance and phase density constraints on early differentiation of chondritic mantle. *Earth Planet. Sci. Lett.* **90**, 144–156. (doi:10.1016/0012-821X(88)90097-0)

Agee, C. B. & Walker, D. 1988*b* Static compression and olivine flotation in ultrabasic silicate liquid. *J. Geophys. Res.* **93**, 3437–3449. (doi:10.1029/JB093iB04p03437)

Agee, C. B. & Walker, D. 1993 Olivine flotation in mantle melt. *Earth Planet. Sci. Lett.* **114**, 315–324. (doi:10.1016/0012-821X(93)90033-6)

Bercovici, D. & Karato, S. 2003 Whole-mantle convection and the transition-zone water filter. *Nature* **425**, 39–44. (doi:10.1038/nature01918)

Berryman, J. G. 2000 Seismic velocity decrement ratios for regions of partial melt in the lower mantle. *Geophys. Res. Lett.* **27**, 421–424. (doi:10.1029/1999GL008402)

Bertka, C. M. & Fei, Y. 1998 Density profile of an SNC model Martian interior and the moment-of-inertia factor of Mars. *Earth Planet. Sci. Lett.* **157**, 79–88. (doi:10.1016/S0012-821X(98)00030-2)

Bottinga, Y. & Weill, D. F. 1970 Densities of liquid silicate systems calculated from partial molar volumes of oxide components. *Am. J. Sci.* **269**, 169–182.

Burnham, C. W. & Davis, N. F. 1971 The role of H_2O in silicate melts. I. *P–V–T* relations in the system $NaAlSi_3O_8$–H_2O to 10 kilobars and 1000°C. *Am. J. Sci.* **270**, 54–79.

Circone, S. & Agee, C. B. 1996 Compressibility of molten high-Ti mare glass; evidence for crystal–liquid density inversions in the lunar mantle. *Geochim. Cosmochim. Acta* **60**, 2709–2720. (doi:10.1016/0016-7037(96)00117-2)

Delano, J. W. 1990 Buoyancy-driven melt segregation in the Earth's Moon, 1. Numerical results. *Proc. 20th Lunar and Planetary Science Conf., Lunar and Planetary Institute, Houston, TX*, pp. 3–12.

Herzberg, C. T. 1984 Chemical stratification in the silicate Earth. *Earth Planet. Sci. Lett.* **67**, 249–260. (doi:10.1016/0012-821X(84)90120-1)

Herzberg, C. T., Baker, M. B. & Wendlandt, R. F. 1982 Olivine flotation and settling experiments on the join Mg_2SiO_4–Fe_2SiO_4. *Contrib. Mineral. Petrol.* **80**, 319–323. (doi:10.1007/BF00378004)

Lange, R. A. & Carmichael, I. S. E. 1987 Densities of Na_2O–K_2O–CaO–MgO–FeO–Fe_2O_3–Al_2O_3–TiO_2–SiO_2 liquids: new measurements and derived partial molar properties. *Geochim. Cosmochim. Acta* **51**, 2931–2946. (doi:10.1016/0016-7037(87)90368-1)

Leahy, G. M. & Bercovici, D. 2007 On the dynamics of a hydrous melt layer above the transition zone. *J. Geophys. Res. Solid Earth* **112**, B07401. (doi:10.1029/2006JB004631)

Matsukage, K. N., Jing, Z. C. & Karato, S. 2005 Density of hydrous silicate melt at the conditions of Earth's deep upper mantle. *Nature* **438**, 488–491. (doi:10.1038/nature04241)

Miller, G. H., Stolper, E. M. & Ahrens, T. J. 1991*a* The equation of state of a molten komatiite, 1, Shock wave compression to 36 GPa. *J. Geophys. Res.* **96**, 11 831–11 848. (doi:10.1029/91JB01204)

Miller, G. H., Stolper, E. M. & Ahrens, T. J. 1991*b* The equation of state of molten komatiite, 2, Application to komatiite petrogenesis and the Hadean mantle. *J. Geophys. Res.* **96**, 11 849–11 864. (doi:10.1029/91JB01203)

Nisbet, E. G. & Walker, D. 1982 Komatiites and the structure of the Archean mantle. *Earth Planet. Sci. Lett.* **60**, 105–113. (doi:10.1016/0012-821X(82)90025-5)

Nolet, G. & Zielhuis, A. 1994 Low S velocities under the Tornquist–Tesseyre zone: evidence for water injection into the transition zone by subduction. *J. Geophys. Res.* **99**, 15 813–15 820. (doi:10.1029/94JB00083)

Ochs, F. A. & Lange, R. A. 1999 The density of hydrous magmatic liquids. *Science* **283**, 1315–1317. (doi:10.1126/science.283.5406.1314)

Ohtani, E. 1984 Generation of komatiite magma and gravitational differentiation in the deep upper mantle. *Earth Planet. Sci. Lett.* **67**, 261–272. (doi:10.1016/0012-821X(84)90121-3)

Ohtani, E. 1985 The primordial terrestrial magma ocean and its implication for stratification of the mantle. *Phys. Earth Planet. Inter.* **38**, 70–80. (doi:10.1016/0031-9201(85)90123-2)

Ohtani, E. & Maeda, M. 2001 Density of basaltic melt at high pressure and stability of the melt at the base of the lower mantle. *Earth Planet. Sci. Lett.* **193**, 69–75. (doi:10.1016/S0012-821X(01)00505-2)

Revenaugh, J. & Sipkin, S. A. 1994 Seismic evidence for silicate melt atop the 410-km mantle discontinuity. *Nature* **369**, 474–476. (doi:10.1038/369474a0)

Rigden, S. M., Ahrens, T. J. & Stolper, E. M. 1984 Densities of liquid silicates at high pressures. *Science* **226**, 1071–1074. (doi:10.1126/science.226.4678.1071)

Rigden, S. M., Ahrens, T. J. & Stolper, E. M. 1989 High-pressure equation of state of molten anorthite and diopside. *J. Geophys. Res.* **94**, 9508–9522. (doi:10.1029/JB094iB07p09508)

Rost, S., Garnero, E. J., Williams, Q. & Manga, M. 2005 Seismological constraints on a possible plume root at the core–mantle boundary. *Nature* **435**, 666–669. (doi:10.1038/nature03620)

Sakamaki, T., Suzuki, A. & Ohtani, E. 2006 Stability of hydrous melt at the base of the Earth's upper mantle. *Nature* **439**, 192–194. (doi:10.1038/nature04352)

Smith, J. R. & Agee, C. B. 1997 Compressibility of molten 'green glass' and crystal–liquid density crosssovers in low-Ti lunar magma. *Geochim. Cosmochim. Acta* **61**, 2139–2145. (doi:10.1016/S0016-7037(97)00055-0)

Stolper, E. M., Walker, D., Hager, B. H. & Hays, J. F. 1981 Melt segregation from partially molten source regions: the importance of melt density and source region size. *J. Geophys. Res.* **86**, 6261–6271. (doi:10.1029/JB086iB07p06261)

Suzuki, A., Ohtani, E. & Kato, T. 1995 Flotation of diamond in mantle melt at high pressure. *Science* **269**, 216–218. (doi:10.1126/science.269.5221.216)

Toffelmier, D. A. & Tyburczy, J. A. 2007 Electromagnetic detection of a 410-km-deep melt layer in the southwestern United States. *Nature* **447**, 991–994. (doi:10.1038/nature05922)

Vidale, J. E. & Hedlin, M. A. H. 1998 Evidence for partial melt at the core–mantle boundary north Tonga from the strong scattering of seismic waves. *Nature* **391**, 682–685. (doi:10.1038/35601)

Vinet, P., Rose, J. H., Ferrante, J. & Smith, J. R. 1989 Universal features of the equation of state of solids. *J. Phys. Condens. Matter* **1**, 1941–1963. (doi:10.1088/0953-8984/1/11/002)

Walker, D. & Hays, J. F. 1977 Plagioclase flotation and lunar crust formation. *Geology* **5**, 425–428. (doi:10.1130/0091-7613(1977)5<425:PFALCF>2.0.CO;2)

Williams, Q. & Garnero, E. J. 1996 Seismic evidence for partial melt at the base of Earth's mantle. *Science* **273**, 1528–1530. (doi:10.1126/science.273.5281.1528)

Yoder, C. F., Konopliv, A. S., Yuan, D. N., Standish, E. M. & Folkner, W. M. 2003 Fluid core size of Mars from detection of the solar tide. *Science* **300**, 299–303. (doi:10.1126/science.1079645)